Journal of Inorganic and General Chemistry
ZAAC
Zeitschrift für anorganische und allgemeine Chemie
doi.org/10.1002/zaac.202100196
ARTICLE

Sterically Encumbered Coordination Sites. Iron(II) Complexes of Jäger-type ligands with a Terphenyl Backbone

Andreas Dürrmann,[a] Gerald Hörner,[a] Stefan Wagner,[b] Matthias Breuning,[b] and Birgit Weber*[a]

Dedicated to Professor Josef Breu on the Occasion of his 60th Birthday

A Schiff base-like ligand $\mathbf{H_2L^{TerPh}}$ featuring a *para*-terphenyl backbone was synthesized and converted in two steps to an octahedral iron(II) coordination polymer with 1,2-bis-(4-pyridyl)-ethylene as bridging ligand. Single crystal X-ray structure analysis was possible for the free ligand and the two octahedral iron(II) complexes. The Schiff base-like ligand features a $[N_2O_2]^{2-}$ coordination sphere for the metal center and the *para*-terphenyl backbone introduces intrinsic steric constraint. Characterization of the coordination polymer with an N_4O_2 coordination sphere around the iron center *via* magnetic measurements (SQUID) and room temperature Mössbauer spectroscopy revealed HS character in the entire temperature range investigated. Structure modelling with DFT calculations supports the findings, but support also the possibility of spin crossover in solution.

Introduction

The discovery of anomalous magnetic behaviour in 3d metal complexes in 1931[1] and the implementation of ligand field theory in the coordination chemists' community in the 1950s paved the way for a new field of research. Nowadays, the observations made by Cambi and Szegö on iron(III) complexes are ascribed to the spin crossover (SCO) phenomenon.[2] The essence of spin crossover is the molecular bistability that refers to the switching between different electronic states in the same metal ion triggered by extrinsic parameters.[3,4] Stimulation of physical parameters such as temperature[5,6] or pressure change,[7] or light-irradiation[5,8] can induce the SCO.

In this context, octahedral iron(II) based complexes are the most extensively studied SCO system,[3,9,10] since their electronic properties allow the change between the paramagnetic high-spin ($S=2$) and diamagnetic low-spin ($S=0$) state which translates into "on-off" from a practical point of view. Thus, spin crossover compounds represent a highly attractive class of molecular magnetic material with potential in future applications in sensors or devices as the magnetism changes as a function of physical parameters allowing direct readout.[11,12] Additionally, merging SCO properties with other attributes is a highly desirable goal in today's materials science to achieve multifunctionality.[10,11,13] Despite a vast number of studies on spin crossover systems, no clear recipe for the "SCO-on-demand" material can be given. It is not possible to reliably predict the transition curve (gradual, abrupt, hysteresis) and whether SCO occurs at all. Contrary to SCO in solution, where the transition usually obeys Boltzmann statistics and can be correlated with DFT modelling,[14,15] the complete understanding of the interplay of molecular properties and intermolecular interactions in the solid-state remains difficult. Consensus, however, exists about the need of intermolecular interactions; so, the synergy between long- and short-range contacts such as hydrogen bonding and linkage of metal centers via bridging ligands seems to be the key towards cooperative spin transitions which are abrupt or even show thermal bistability (hysteresis).[16,17]

A widely investigated SCO system using N_2O_2 coordinating Schiff base-like ligands derives from the *ortho*-phenylenediamine backbone.[18,19] From this parent compound, several Schiff Base-like ligands with a N_2O_2 coordination sphere and their iron (II) complexes were prepared and described in detail. Although members of this family were reported with modifications in position 4 and 5, like long alkyl chains for lipid-layer structures,[20] or extended aromatic systems with interesting luminescent properties,[21,22] there is not yet an example with moieties in the 3 and/or 6 position. In this work, a new prototype of such ligands carrying two phenyl rings in those positions is presented along with its methanol complex and an iron(II) coordination polymer. The ligand is based on *para*-

[a] A. Dürrmann, Dr. G. Hörner, Prof. Dr. B. Weber
Department of Chemistry, Inorganic Chemistry
University of Bayreuth
Universitätsstraße 30, NWI, 95440 Bayreuth, Germany
E-mail: weber@uni-bayreuth.de
[b] S. Wagner, Prof. Dr. M. Breuning
Department of Chemistry, Organic Chemistry
University of Bayreuth
Universitätsstraße 30, NWII, 95440 Bayreuth, Germany

Supporting information for this article is available on the WWW under https://doi.org/10.1002/zaac.202100196

terphenyl and represents the first type of Schiff Base-like ligands with functionalization in the [3,6] position (Scheme 1).

Results and Discussion

Synthesis

Ligand precursor **3** (1,2-diamino-3,6-diphenyl-benzene) was prepared in three steps from readily and commercially available 2,1,3-benzothiadiazole **1** according to known procedures[23] (Scheme 1). Regioselective diiodination of **1** in positions 4 and 7 followed by Suzuki reaction with phenyl boronic acid afforded the diphenyl-substituted benzothiadiazole **2**. This compound was subjected to reductive sulfur extrusion with $NaBH_4$ in the presence of catalytic amounts of $CoCl_2$, which provided the terphenyl diamine **3** with high purity. Condensation of **3** with two equivalents of 3-methoxymethylene-2,4-pentanedione yielded the analytically pure ligand $\mathbf{H_2L^{TerPh}}$. Elemental analysis, mass spectrometry as well as proton NMR spectroscopy confirmed the identity. The molecular structure was studied in detail by X-ray structure analysis of single crystals of $\mathbf{H_2L^{TerPh}}$ obtained from methanol (*vide infra*).

^{1}H-NMR spectra of the ligand $\mathbf{H_2L^{TerPh}}$ were recorded of diluted solutions in $CDCl_3$ at 300 MHz and 500 MHz. Similar to the unsubstituted phenylenediamine-derived ligand $\mathbf{H_2L}$, $\mathbf{H_2L^{TerPh}}$ adopts a ketoenamine structure. In both cases the signal at lowest field, $\delta = 12.5$ ppm, is split to a doublet ($J = 12.3$ Hz) through vicinal coupling with the ene proton. This pattern can be readily distinguished from the complementary imine enol form which is expected to give a broad singlet for the phenolic proton at even lower field. While the conserved chemical shift of the amine proton of $\mathbf{H_2L^{TerPh}}$ in comparison to that of the reference ligand $\mathbf{H_2L}$ with no substituent in [3,6] position indicates an only minor effect of remote substitution on the electronic properties of the ligand as a whole, feedback of the terphenyl backbone can be read from the marked upfield shift of the ene proton resonance in $\mathbf{H_2L^{TerPh}}$ (Figure 1). While this signal is located at 8.1 ppm for $\mathbf{H_2L}$[24] it is shifted to ca. 7.4 ppm in $\mathbf{H_2L^{TerPh}}$ where it is convoluted with the resonances of the aromatic protons. This high-field shift indicates an influence of the outer phenyl rings which can be interpreted in terms of an aromatic ring current. The structure of $\mathbf{H_2L^{TerPh}}$ in the crystal indeed features close contacts of the ene sites and the outer phenyl rings. In solution, rotation of the ligand arms in $\mathbf{H_2L^{TerPh}}$ is most likely hindered due to the presence of the phenyl rings. As a matter of fact, the appearance of the NMR spectra of $\mathbf{H_2L^{TerPh}}$ is clearly affected by the frequency used in the NMR experiment. The spectra recorded at 300 MHz show better defined peaks compared to the 500 MHz spectra (Figures S1–S3).

Reaction of $\mathbf{H_2L^{TerPh}}$ with iron(II) acetate in methanol yielded a red-brown colored solution indicating the formation of $\mathbf{[Fe(L^{TerPh})(MeOH)_2]}$. The isolation of bulk quantities of the methanol complex proved challenging. A small batch of the powdered product was isolated directly from the reaction mixture and was identified as $\mathbf{[Fe(L^{TerPh})(MeOH)_2]}$ by means of elemental analysis. Keeping the concentrated solution at room temperature for several days gave a small fraction of brown crystals which were identified as $\mathbf{[Fe(L^{TerPh})(MeOH)_2]\cdot 3(MeOH)}$ by X-ray structure analysis (*vide infra*). Attempts were made to receive the corresponding pyridine complex $\mathbf{[Fe(L^{TerPh})(py)_2]}$ analogous to the reported parent complex $\mathbf{[Fe(L)(py)_2]}$.[25] However, vapor diffusion of diethyl ether into a methanol/pyridine solution that contained $\mathbf{H_2L^{TerPh}}$ and $Fe(OAc)_2$ gave a crystalline product only after prolonged standing (about 1 month). X-ray analysis of the received large yellow crystals revealed complete oxidation of iron to give the well-known acetato-bridged Fe_{10} wheel.[26] By contrast, a coordination

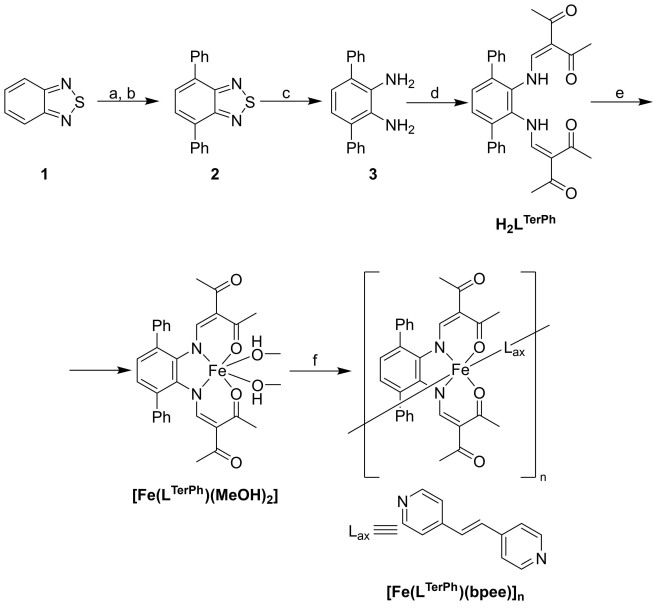

Scheme 1. Synthesis of the ligand and the complexes described in this work. a) I_2, Ag_2SO_4, H_2SO_4, Δ, 66 %; b) $PhB(OH)_2$, $Pd(PPh_3)_4$, K_2CO_3, toluene, H_2O, 90 °C, 75 %; c) $NaBH_4$, $CoCl_2\cdot 6\,H_2O$, EtOH, THF, Δ, 76 %; d) 3-methoxymethylene-2,4-pentanedione, MeOH, Δ, 55 %; e) $Fe(OAc)_2$, MeOH, Δ; f) 4,4′-bpee, RT.

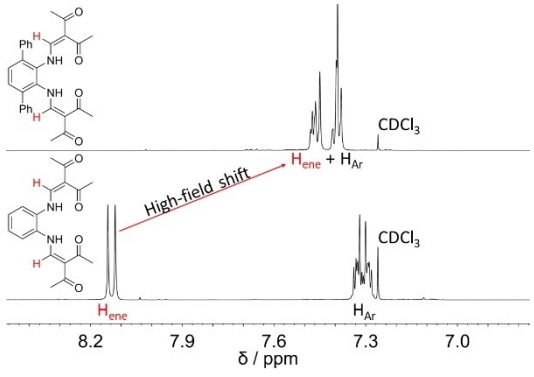

Figure 1. Excerpt of the aromatic region in the ^{1}H NMR spectra of $\mathbf{H_2L^{TerPh}}$ (top) and $\mathbf{H_2L}$ (bottom). Spectra were recorded at 298 K and 500 MHz. The ene proton is highlighted in red. The signal of the solvent (chloroform) is indicated.

Table 1. Crystallographic data for the compounds H_2L^{TerPh}, $[Fe(L^{TerPh})(MeOH)_2]\cdot 3$ **(MeOH)** and $[Fe(L^{TerPh})(bpee)]_n$ presented in this work.

	H_2L^{TerPh}	$[Fe(L^{TerPh})(MeOH)_2]\cdot 3$ (MeOH)	$[Fe(L^{TerPh})(bpee)]_n$
CCDC number	2086357	2086358	2086359
Formula	$C_{30}H_{28}N_2O_4$	$C_{35}H_{46}Fe_1N_2O_9$	$C_{42}H_{36}Fe_1N_4O_4$
Sum formula	$C_{30}H_{28}N_2O_4$	$C_{32}H_{34}Fe_1N_2O_6$, $3\times C_1H_4O_1$	$C_{30}H_{26}Fe_1N_2O_4$, $C_{12}H_{10}N_2$
M/g·mol^{-1}	480.54	694.59	716.60
Crystal system	triclinic	triclinic	triclinic
Space group	$P\bar{1}$	$P\bar{1}$	$P\bar{1}$
Crystal description	Colourless plate	Brown block	Blue-green column
Crystal size/mm	0.185×0.078×0.075	0.363×0.314×0.280	0.215×0.088×0.042
a/Å	9.8958(5)	10.3524(3)	10.2340(3)
b/Å	10.1400(5)	12.2557(3)	12.6391(4)
c/Å	13.7523(7)	14.5167(4)	14.6591(5)
α/°	102.491(4)	89.640(2)	102.202(3)
β/°	107.561(4)	84.202(2)	95.693(3)
γ/°	94.514(4)	81.014(2)	106.317(2)
V/Å^3	1269.05(12)	1809.82(9)	1753.05(10)
Z	2	2	2
$\rho_{calculated}$/g·cm^{-3}	1.258	1.275	1.358
μ/mm^{-1}	0.084	0.470	0.480
F(000)	508	736	748
θ_{range}/°	3.1–28.4	3.3–28.5	3.6–28.5
Index range (h k l)	$-13\le h\le 5$ $-13\le k\le 13$ $-17\le l\le 18$	$-11\le h\le 13$ $-16\le k\le 16$ $-19\le l\le 17$	$-13\le h\le 5$ $-16\le k\le 16$ $-19\le l\le 19$
γ/Å	Mo–Kα (0.71073)	Mo–Kα (0.71073)	Mo–Kα (0.71073)
T/K	170	170	170
Reflns. coll.	15272	20363	22207
Indep. reflns. (R_{int})	5958 (0.072)	8462 (0.042)	8368 (0.037)
Data/restraints/parameters	5958/0/331	8462/0/435	8368/0/460
$R1$, w$R2$ [$I>2\,\sigma(I)$]	0.0567, 0.1438	0.0544, 0.1676	0.0368, 0.0763
GooF (S)	0.87	1.06	0.90
Min. and Max. $\rho_{residual}$/eÅ^{-3}	−0.25, 0.22	−0.65, 0.95	−0.28, 0.32

polymer based on iron(II) mononuclear units was cleanly obtained via a one-pot method by addition of solid 1,2-bis-(4-pyridyl)-ethylene (4,4′-bpee) to the solution of **[Fe(L^{TerPh})(MeOH)$_2$]**. An immediate color change to dark blue occurred, along with the growth of a small amount of deeply blue-greenish crystals. The structure was determined by X-ray crystallography as **[Fe(L^{TerPh})(bpee)]$_n$** and indicated high-spin character of the metal ion. This assignment is corroborated by room temperature Mössbauer spectroscopy and VT-SQUID magnetometry (see below).

Single crystal X-ray crystallography

Crystals suitable for single crystal X-ray structure analysis of all compounds were picked from the reaction solutions (Figures S4-S6). Crystallographic data, as summarized in Table 1, were collected of **H$_2$L^{TerPh}**, **[Fe(L^{TerPh})(MeOH)$_2$]·3 (MeOH)** and **[Fe(L^{TerPh})(bpee)]$_n$** at 170 K. Asymmetric units with complete atom numbering can be found in the SI, Figures S7-S9.

Ligand **H$_2$L^{TerPh}** crystallizes without any additional solvent molecules in the triclinic system in the space group $P\bar{1}$ (Figure 2). While Schiff base ligands exist either as keto-enamine or enol-imine tautomer, the bond lengths in **H$_2$L^{TerPh}** are

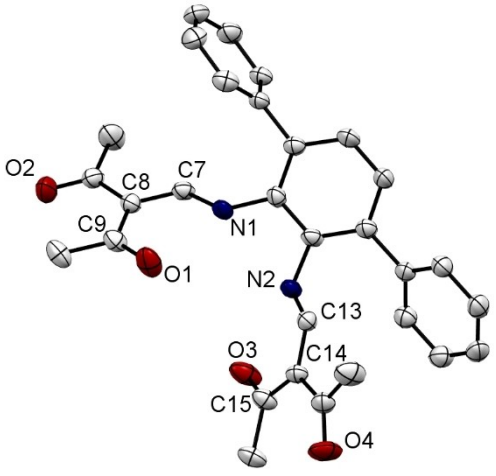

Figure 2. Structure of **H$_2$L^{TerPh}** in the crystal. Hydrogen atoms are omitted for clarity. Thermal ellipsoids are drawn at 50 % probability level.

indicative of the keto-enamine species (d(C7–C8/C13–C14) = 1.38 Å and d(C8–C9/C14–C15) = 1.46 Å), in accordance with observations from NMR spectroscopy.[27] Intramolecular hydrogen bonding (>C=O···HN<) enforces planarity within the

keto-enamine group of each ligand arm. The planes of the keto-enamine moieties are tilted from mutual co-planarity as they deviate from co-planarity with the plane of the central phenyl ring. The terphenyl backbone shows gauche conformation of the terminal phenyl rings, what supports several C–H···π interactions in the solid state, both intramolecularly and intermolecularly. An intramolecular contact prevails between the ene proton H7 and one terminal phenyl ring. This situation reflects in the site-selective high-field shifts in NMR.

Packing of **H_2L^{TerPh}** comprises classic hydrogen bonding between the enamine proton and the carbonyl group (N2–H2···O3) resulting in pairs of ligand molecules (Figure 3). By contrast, there are no significant π–π contacts (distance between phenyl planes >5 Å), in spite of the presence of the *para*-terphenyl moiety. Additional C–H···π contacts cause a stacked array of those pairs in the crystallographic *a*-direction. Non-classical hydrogen bonding[28] between a methyl group and carbonyl oxygen atom C18–H18 A···O4 completes the packing and connects the stacked ligand pairs.

Both iron(II) compounds, **[Fe(L^{TerPh})(MeOH)$_2$]·3 (MeOH)** and **[Fe(L^{TerPh})(bpee)]$_n$**, crystallize in the triclinic system in the space group $P\bar{1}$. In the case of the methanol complex, the asymmetric unit consists of the octahedral complex with two methanol molecules as axial ligands along with three non-coordinating MeOH molecules (Figure 4a). The coordination polymer crystallizes without additional solvent molecules in the crystal packing. As is commonly seen with coordination polymers of this type, the asymmetric unit comprises the N_3O_2-coordinate fragment as the propagation unit (Figure 4b). The iron(II) ions are found in an octahedral environment in both complexes. Pertinent bond distances, bond angles and the octahedral distortion parameters[29] are summarized in Table 2.

While the overall data are indicative of HS-configured iron (II) centers in both complexes, the N_2O_4 environment of **[Fe(L^{TerPh})(MeOH)$_2$]·3 (MeOH)** reveals highly anisotropic axial ligation; that is, the bond lengths of the nominally equivalent Fe-O_{ax} bonds differ by as much as 0.12 Å. This axial distortion in **[Fe(L^{TerPh})(MeOH)$_2$]·3 (MeOH)** goes along with massive deformation of the N_2O_2 equator. The nearly C_s symmetric N_2O_4

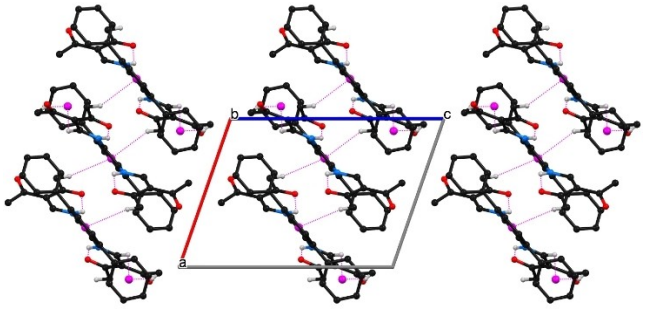

Figure 3. Excerpt of the crystal packing of **H_2L^{TerPh}** along crystallographic axis *b*. Hydrogen atoms not involved in hydrogen bonds are omitted for clarity. Hydrogen bonds and C–H···π interactions are drawn as pink dashed lines.

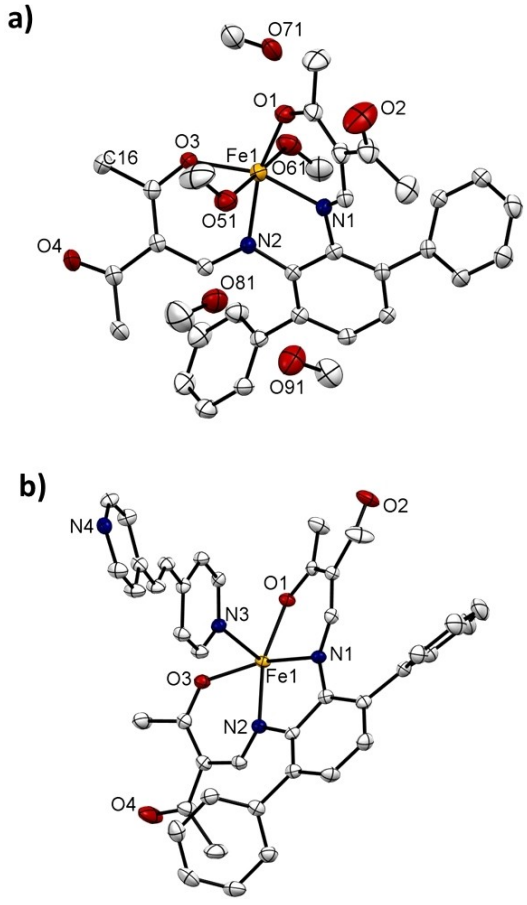

Figure 4. Structure of the asymmetric unit of a) **[Fe(L^{TerPh})(MeOH)$_2$]·3 (MeOH)**; and b) **[Fe(L^{TerPh})(bpee)]$_n$**. Hydrogen atoms are omitted for clarity. Thermal ellipsoids are drawn at 50 % probability level.

Table 2. Selected bond lengths *d*/Å, and angles ∢/° and octahedral distortion parameters within the inner coordination sphere of the coordination compounds.

	[Fe(L^{TerPh})(MeOH)$_2$]·3 (MeOH)	[Fe(L^{TerPh})(bpee)]$_n$
d(Fe1–N1)/Å	2.0777(19)	2.1076(13)
d(Fe1–N2)/Å	2.0905(19)	2.1096(14)
d(Fe1–O1)/Å	2.0029(17)	2.0271(12)
d(Fe1–O3)/Å	1.9950(17)	2.0289(12)
d(Fe1–O51)/Å	2.295(2)	–
d(Fe1–O61)/Å	2.170(2)	–
d(Fe1–N3)/Å	–	2.2690(14)
d(Fe1–N4)/Å	–	2.2799(15)
∢(O51–Fe1–O61)/°	179.09(8)	–
∢(N3–Fe1–N4)/°	–	173.14(5)
∢(O1–Fe1–O3)/°	111.40(7)	113.33(5)
Δ	0.0024	0.0023
θ/°	236.04	292.78
Σ/°	72.82	74.32

coordination sphere is bent downward relative to the phenyl plane and the iron(II) center is dislocated about 0.715 Å beneath this plane. This finding is reminiscent of the solid-state structure reported for a 1,8-diaminonaphthalene iron(II) complex where the metal center is only penta-coordinated and about 0.46 Å out of plane.[30] In the parent system **[Fe(L)(MeOH)$_2$]**, the iron(II) center is likewise displaced from the phenyl plane but to a lesser extent (0.421 Å) while there is no anisotropy of the axial Fe–O bond lengths.[31] Viewing from the front, the chelate resembles a boat or saddle conformation, whereas a side view reveals a significant pyramidalization of the coordinating nitrogen atoms with a N-distance from the C–Fe–C plane of about 0.15 Å. For comparison, other systems exhibit minor pyramidalization[15,19] (distance around 0.03 Å) suggesting that conjugation within the chelate in **[Fe(L^{TerPh})(MeOH)$_2$]·3 (MeOH)** is partially relieved.

With another view on the conformational aspects, the almost ecliptic orientation ($\theta = 16.8°$) of the ring planes of the terphenyl in **[Fe(L^{TerPh})(MeOH)$_2$]·3 (MeOH)** differs from the terphenyl backbone in **[Fe(L^{TerPh})(bpee)]$_n$** that exhibits a gauche conformation ($\theta = 77.1°$), placing the terminal phenyls above and below the coordination plane (Figure 5). This translates into an approximately C_2 symmetric orientation which leaves the N_2O_2 chelate close to planar. Relative to the central phenyl ring drilled coordination arms acquire a chair-like conformation in favor of intact chelate conjugation. Akin to the coordination polymer, this "facing-away" can be observed in the structure of the ligand where the phenyl rings are also gauche, albeit with a reduced dihedral angle ($\theta = 59.6°$). An illustration of this description is given below in Figure 5. The reason, why the chelate ring and the terphenyl tends to occupy a different conformation depending on the axial ligand is not obvious. It appears that the steric repulsion does not differ in a pronounced way among the native ligand and the complexes (compare metrics of intramolecular CH···π interactions in Table 3) suggesting that the increase of internal pressure upon insertion of iron(II) in the chelate pocket is rather small. From this point, one can conclude an intrinsically constrained character in **H$_2$L^{TerPh}**, due to the phenyl substitution.

As expected from the divergent stoichiometry the crystal structures reveal vastly different intermolecular interaction patterns. As described for **H$_2$L^{TerPh}**, π–π contacts do not determine the crystal packing of both iron complexes (distance between phenyl planes > 4 Å). Hydrogen bonding mediated by MeOH is the major contribution to the crystal packing in **[Fe(L^{TerPh})(MeOH)$_2$]·3 (MeOH)** as shown in Figure 6. The net-

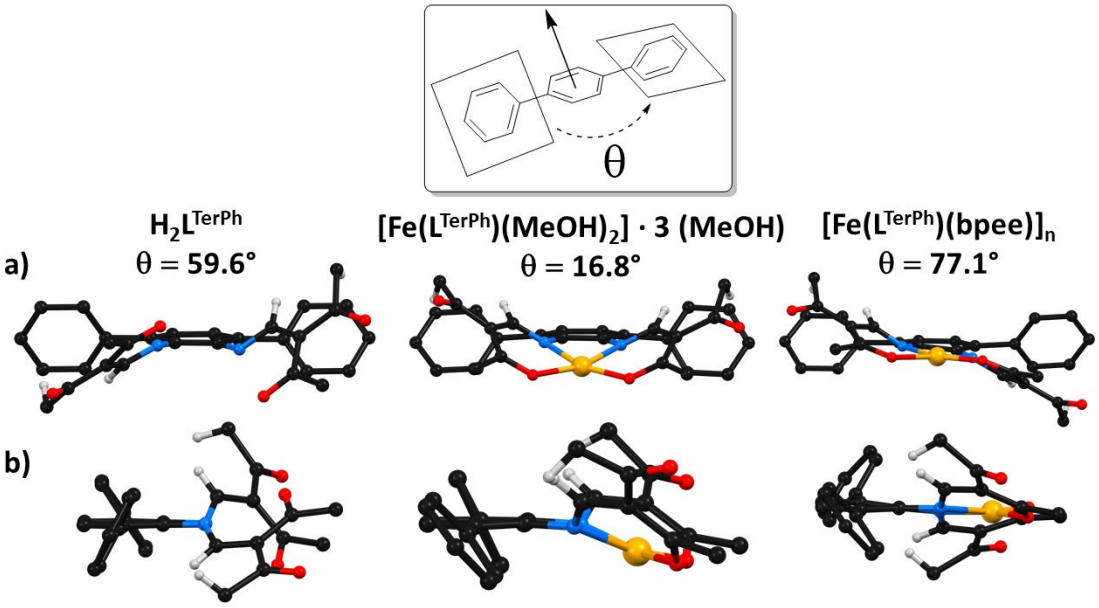

Figure 5. a) Front and b) side view of the compounds **H$_2$L^{TerPh}**, **[Fe(L^{TerPh})(MeOH)$_2$]·3 (MeOH)** and **[Fe(L^{TerPh})(bpee)]$_n$** studied in this work. Hydrogen atoms other than the ene and from the methyl groups pointing towards the phenyl rings are omitted for clarity. Theta θ is defined as the dihedral angle between the terminal phenyl rings.

Table 3. Metrics *d*/Å, and angles ∢/○ of intramolecular hydrogen bonding between the hydrogen of methyl groups and ene proton directing towards the phenyl planes in **[Fe(L^{TerPh})(MeOH)$_2$]·3 (MeOH)** and **[Fe(L^{TerPh})(bpee)]$_n$**.

	$d(H_{Me}\cdots\pi)$/Å	$\sphericalangle(H_{Me}\cdots\pi)$/°	$d(H_{ene}\cdots\pi)$/Å	$\sphericalangle(H_{ene}\cdots\pi)$/°
H$_2$L^{TerPh}	2.968 3.260	158 145	2.973 3.223	124 100
[Fe(L^{TerPh})(MeOH)$_2$]·3 (MeOH)	2.871 3.032	152 154	3.092 3.049	113 118
[Fe(L^{TerPh})(bpee)]$_n$	2.920 2.879	159 160	2.954 3.042	127 118

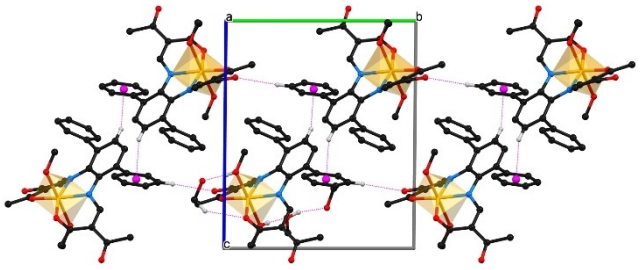

Figure 6. Excerpt of the crystal packing of **[Fe(L^{TerPh})(MeOH)$_2$]·3(MeOH)** viewed along crystallographic axis *a*. Hydrogen atoms not involved in hydrogen bonds are omitted for clarity. Hydrogen bonds, C–H···π and CH···O interactions are drawn as pink dashed lines. Coordination polyhedra are highlighted.

work consists predominantly of hydrogen bonding between methanol molecules and the non-coordinating carbonyl groups. An infinite chain of complex molecules along the crystallographic axis *a* originates from the linkage of the independent complexes by an incorporated solvent (O71–H71···O4, O61–H61···O71). These strains consequently pair-up *via* contact of one phenyl ring and an aromatic proton. Bifurcation of those pairs is the result of further hydrogen bonding between a coordinating methanol and a carbonyl group mediated by two solvent molecules (O51–H51···O81, O81–H81···O91, O91–H91···O2). Finally, weak non-classic contacts between a ketone group and an aromatic proton (C23–H23···O4) are responsible for another strand of complex molecules propagating in the crystal. The bridging ligand *trans*-1,2-bis-(4-pyridyl)-ethylene (4,4′-bpee) links individual units of **[Fe(L^{TerPh})]** to an infinite 1D chain consisting of the coordination polymer **[Fe(L^{TerPh})(bpee)]$_n$** in an AAAA sequence with a Fe–Fe distance of 13.85 Å (Figure 7a); that is, in comparison with similar systems, the usual order of complex units in a polymeric strand.[17,32–34] Recently, an ABAB coordination polymer with **[Fe(L)]** units tilted by 180° was found, having –CF3 groups at the chelate cycle.[35] The Fe–N$_{ax}$ bond length (ca. 2.2 Å) is comparable to similar bond lengths in other reported coordination polymers,[32,36] as is the torsion angle between the pyridyl rings with 20.3°.[33]

Considering the molecular packing, the individual one-dimensional chains build up to pairs via C–H···π interactions. The array of the chains becomes evident by the highlighted coordination polyhedra shown in the perpendicular view to the *bc*-plane (Figure 7b). Further intermolecular contacts are identified as the interaction between the olefinic hydrogen atoms of 4,4′-bpee and non-coordinating carbonyl oxygen atoms (C41–H···O4 and C42–H42···O2).

Spin states in the solid and in solution

As iron(II) complexes of the Jäger type ligands are generally highly susceptible towards oxidation and only a small amount of **[Fe(L^{TerPh})(bpee)]$_n$** was available, the bulk material was embedded into an inert matrix of a fluorinated polymer to

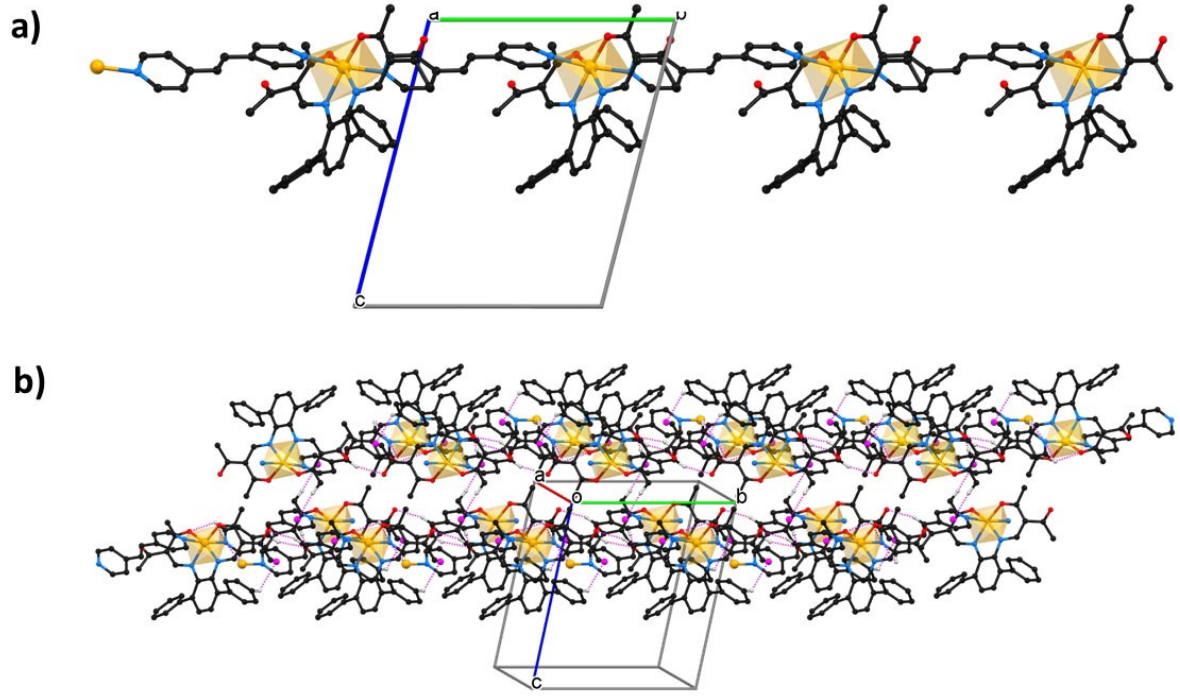

Figure 7. View onto an excerpt of the crystal packing of **[Fe(L^{TerPh})(bpee)]$_n$** at perpendicular view to *bc* plane. Hydrogen atoms not involved in hydrogen bonds are omitted for clarity. Hydrogen bonds, C–H···π and CH···O interactions are drawn as pink dashed lines. Coordination polyhedra are highlighted.

suppress oxidation processes. SQUID magnetometry data were recorded of the coordination polymer between 400–50 K at an applied field of 5000 Oe and 5 K·min^{-1} scan rate. There is no evidence of SCO behavior in this compound and the iron(II) center remains in the HS state over the given temperature range (Figure 8a). The magnetic susceptibility-temperature product at room temperature with 3.40 cm^{3}Kmol^{-1} is clearly in the range for other reported HS iron(II) compounds.[18] Room temperature ^{57}Fe Mössbauer spectroscopy of **[Fe(L^{TerPh})(bpee)]$_n$** unveiled the presence of only one iron(II) site with $S=2$. The observed doublet shown in Figure 8b and the derived Mössbauer parameters match with reported values for the assumed iron(II) high spin species.[25,37] Additionally, no iron-containing impurity or oxidation product can be observed.

While the temperature-invariant susceptibility of **[Fe(L^{TerPh})(bpee)]$_n$** indicates that the iron(II) center of the coordination polymer does not change its spin state at all and conserves the HS state irrespective of temperature, this conclusion reasonably applies to the solid state only. In particular, it does not rule out SCO of the isolated molecule/polymer strand in solution. As a matter of fact, dipping the dilute filtrate of **[Fe(L^{TerPh})(bpee)]$_n$** into liquid nitrogen results in a color change from faint orange-brownish to intensely blue, indicative of SCO in solution/glass, if at very low temperature (Figure 9a).

While the coordination polymer **[Fe(L^{TerPh})(bpee)]$_n$** with $N_4O_{\bar{a}2}$ coordinate iron exhibits blue-green color in the solid-state, a diluted solution of this compound in MeOH appears orange-brownish at room temperature. This discrepancy must be associated with a changed coordination in solution from N_4O_2 to N_3O_3 and/or N_2O_4, as disruption of the polymer will leave open coordination sites that can be filled by the solvent methanol; it is noted that color remains unaffected even upon addition of a large excess of 4,4′-bpee. In keeping with a (fractional) coordination of MeOH, solutions of the isolated methanol-coordinated iron(II) precursor are similarly colored at room temperature. Importantly, however, these solutions do not show any color evolution at low temperature. Therefore we conclude that the intense blue color observed in frozen solutions of **[Fe(L^{TerPh})(bpee)]$_n$** requires the presence of both, iron(II) and the bridging ligand. Accordingly, the temperature-dependent color change of diluted solutions of **[Fe(L^{TerPh})(bpee)]$_n$** in MeOH can be associated with either or both, varied axial coordination and spin-state variation.

In order to receive more insight into the speciation in solution, room temperature UV-Vis spectra of the filtrate were recorded (Figure S11, SI). They show intense absorption in the near-UV range and significant absorption across the entire Vis regime which successively decreases towards the NIR region. We used TD-DFT methods to assign the color at room temperature to the possible species. Included in Figure 9b are spectra which derive from TD-DFT computation of several reasonable

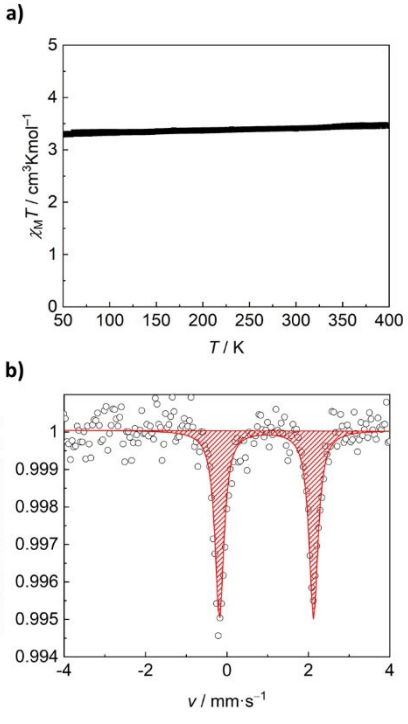

Figure 8. a) Plot of $\chi_M T$ vs. T over the range 400–50 K for the scan rate of 5 Kmin^{-1} at an applied field of 5000 Oe for the complex **[Fe(L^{TerPh})(bpee)]$_n$**. b) Room temperature ^{57}Fe Mössbauer spectrum of **[Fe(L^{TerPh})(bpee)]$_n$**. The HS doublet is drawn in red color. Mössbauer parameters: $\delta=0.97(1)$ mm·s^{-1}, ⊠$E_Q=2.31(2)$ mm·s^{-1}, $\Gamma=0.13(2)$ mm·s^{-1}.

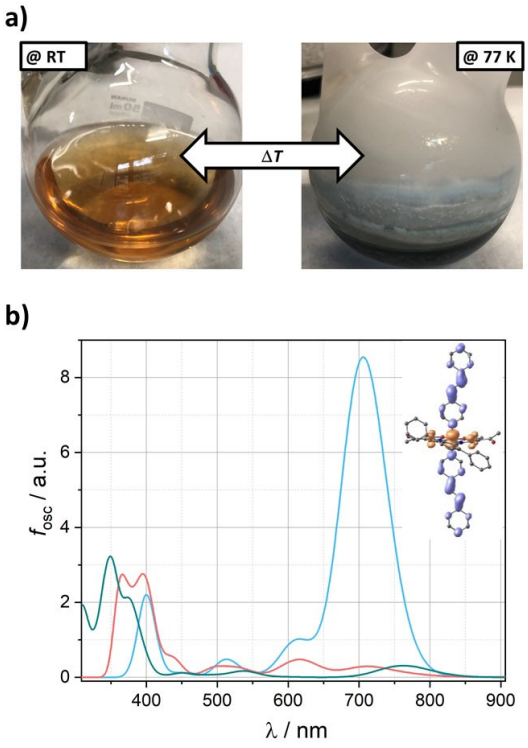

Figure 9. a) Colour change of the filtrate of **[Fe(L^{TerPh})(bpee)]$_n$ in MeOH** upon cooling from room temperature to liquid nitrogen temperature; b) TD-DFT derived optical spectra of **HS-[Fe(L^{TerPh})(MeOH)$_2$]** (green), **HS-[Fe(L^{TerPh})(bpee)$_2$]** (red) and **LS-[Fe(L^{TerPh})(bpee)$_2$]** (blue); inset: difference density of the leading NIR-transition of **LS-[Fe(L^{TerPh})(bpee)$_2$]** (red: source; blue: sink).

constituents (TPSSh/TZVP; mononuclear models of the polymers were used). Both HS-species (axial ligand: MeOH or 4,4′-bpee) give spectra that are in qualitative agreement with the measured spectra; intense near-UV transitions give rise to a tailing throughout the visible range which is superimposed by additional transitions.

Obviously only the spectrum of **LS-[Fe(L^{TerPh})(bpee)$_2$]** (blue in Fig. 9b) captures the observed color at low temperatures qualitatively and quantitatively. The intense transition has clear metal-to-ligand charge transfer character, with the π-system of axial 4,4′-bpee providing strong acceptor levels (Figure 9b, inset). Comparison of the frontier MO diagrams of **LS-[Fe(L^{TerPh})(bpee)$_2$]**, **LS-[Fe(L^{TerPh})(py)$_2$]** and **LS-[Fe(L^{REF})(py)$_2$]** corroborates the crucial importance of the enlarged axial π-system (see Figure S10, SI). Besides intercalating the acceptor levels of the MO diagram, 4,4′-bpee tends to stabilize also the three highest metal-borne donor levels (*t_{2g}* like) by 100–150 mV. By contrast, the native terphenyl backbone only marginally affects the electronic structure; for instance, the TerPh-borne LUMO + 1 is located ca. 200 mV above the LUMO of **[Fe(L^{TerPh})(py)$_2$]**, but can be expected to become spectroscopically and chemically relevant upon further stabilization. Future work will address further modification of the terphenyl π-system with electron-withdrawing substituents.

Theoretical Modelling of SCO Energies

As seen in the above, oligomers of **[Fe(L^{TerPh})(bpee)]$_m$** (with $m \ll n$) will undergo SCO in solution, close to liquid nitrogen temperatures, whereas its HS-state is trapped in the solid even at lowest temperatures. In order to get insights into the feedback of ligand sterics on SCO energetics, we have addressed the system with means of density-functional theory. Optimised structures are in good agreement with experimental metrics as far as available. Pertinent metrics of the optimised structures are summarised in Table S7, SI.

$$\boxtimes_{SCO}E = \boxtimes_{SCO}E^0 + (\delta_{SCO}E \times a_0) \quad (1)$$

Reliable relative SCO energies, $\boxtimes_{SCO}E$, extracted from *Fock-exchange scans* (equ. 1) which were elaborated by Jakubikova et al.[38,39] The slopes of these plots have been previously shown to be structure-independent within a family of complexes. By contrast, the offset of the plots will reflect the structure-bias of the SCO energies. Such derived plots are shown in Figure 10. We were pleased to find only a marginal effect of the terphenyl backbone on the SCO energies. In fact, values of $\boxtimes_{SCO}E$ obtained for **[Fe(L^{TerPh})(py)$_2$]** and **[Fe(L^{REF})(py)$_2$]** are hardly discernible (blue and red in Figure 10). By contrast, variation of the axial ligand affects the SCO energies. The strongly destabilized LS–state of **[Fe(L^{TerPh})(MeOH)$_2$]** reflects the weak-field character of MeOH (black in Figure 10). Somewhat surprisingly, also 4,4′-bpee as an axial ligand is predicted to weaken the overall ligand-field, concomitant with significantly smaller SCO energies relative to pyridine, with $\boxtimes\boxtimes_{SCO}E \approx -10$ kJ mol^{-1}.

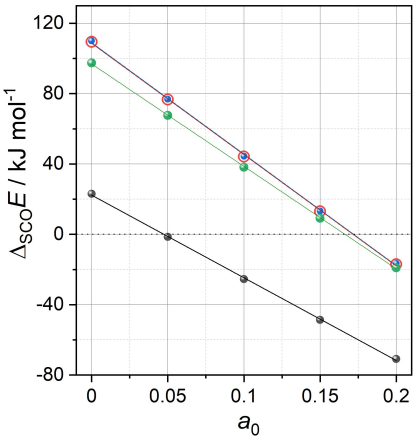

Figure 10. DFT-derived (B3LYP–D/TZVP) apparent SCO energies of iron(II) complexes as a function of the amount of exact Fock-exchange a_0; red: **[Fe(L^{REF})(py)$_2$]**; blue: **[Fe(L^{TerPh})(py)$_2$]**; green: **[Fe(L^{TerPh})(bpee)$_2$]**; black: **[Fe(L^{TerPh})(MeOH)$_2$]**.

Conclusions

In this work we reported the synthesis and characterization of a new Schiff base-like ligand with phenyl substituents in [3,6]-position of the phenylene backbone. Although the terphenyl unit features geometrical constraint, they do satisfactorily queue into the related *ortho*-phenylenediamine family of Schiff base-like Jäger-type ligands and are of huge interest for future studies. Indeed, although for the corresponding iron(II) coordination polymer no spin crossover behaviour is observed in the solid state, investigations in solution in combination with theoretical modelling indicate, that the realization of the desired properties is in principle possible.

Experimental Section

Materials and Methods

Iron(II) acetate[40] and 3-methoxymethylene-2,4-pentanedione[41] were prepared according to literature. All other chemicals were commercially available and used as received. Methanol was distilled over Mg prior to use.[42] Air-sensitive preparations were carried out under Argon 5.0 atmosphere using Schlenk tube techniques. NMR spectra were recorded with a 500 MHz Avance III HD and a 300 MHz Avance 300 spectrometer from Bruker. CHN analyses were performed with an Unicube from Elementar AnalysenSysteme. The samples were weighed into a tin boat with sulfanilamide as reference. Mass spectra were recorded with a Finnigan MAT 8500 with a data system MASPEC II. X-ray Structure Analysis was performed with a Stoe StadiVari diffractometer using graphite-mono-chromated Mo-K_α radiation. The data were corrected for Lorentz and polarisation effects. The structures were solved by direct methods (SHELXT[43]), refined by full-matrix least-square techniques against F_o^2–F_c^2 (SHELXL-2018/3[44]), and interfaced by WinGX.[45] *N*-bonded hydrogen atoms were refined with free N–H distance; all other hydrogen atoms of were calculated in idealised positions with fixed displacement parameters during refinement. Mercury[46] was used for structure illustrations and Platon[47] for

computing structural data. Octahedral distortion parameters were calculated using OctaDist.[29] Magnetic measurements were carried out using a SQUID MPMS-XL5 magnetometer from Quantum Design. A magnetic field of 5000 Oe was applied, and the samples were measured in the range from 400 to 50 K in sweep mode (5 K·min^{-1}). The samples were placed in a gelatine capsule held in a plastic straw. The raw data was corrected for the diamagnetism of the sample holder and the organic ligand using tabulated Pascal's constants.[48] ^{57}Fe Mössbauer spectra were recorded in transmission geometry in a constant-acceleration mode using a conventional Mössbauer spectrometer equipped with a 50 mCi ^{57}Co(Rh) source. The spectra were fitted using Recoil 1.05 Mössbauer Analysis Software.[49] The isomer shifts were reported with respect to α-Fe as a reference at room temperature.

Computational Details

DFT calculations were performed using ORCA2.9.1.[50] Large TZVP basis sets[51] were used throughout. The structures of the iron(II) complexes were optimized with the GGA functional BP86.[52] Complexes were optimized in both their LS and HS states. Cartesian coordinates of all optimized structures are compiled in the Supporting Information (Tables S8–S13). Molecular orbitals and electronic properties were extracted from single-point calculations in the optimised positions with the global hybrid functional TPSSh.[53] These settings provide reliable optical transition energies as shown recently for planar nickel(II)[21,54] and octahedral iron(II) complexes.[55] In order to assess the SCO energies, we used five derivatives of the well-established hybrid functional B3LYP[39,56] in single-point calculations. In these derivative functionals the amount of exact exchange a_0 has been varied stepwise from 0.20 (native B3LYP) to 0.00. Dispersion contributions were approximated using Grimme's DFT–D3 atom pairwise dispersion corrections of the parent B3LYP functional.[57] Solvent effects were accounted for in a dielectric continuum approach (COSMO),[58] parametrized for MeCN.

H_2L^{TerPh}: To a suspension of crude terphenyl diamine (0.30 g, 1.2 mmol, 1.0 Eq.) in methanol (20 mL) is added a solution of 3-methoxymethylene-2,4-pentanedione (0.61 g, 4.3 mmol, 3.7 Eq.) in methanol (2 mL). The resulting yellow solution is refluxed for one hour. Upon cooling to RT, a colorless solid precipitated, which contained crystals suitable for X-ray structure analysis that were separated along with some mother liquor. The supernatant solution was concentrated in vacuo to the half of the original volume and stored at −30 °C for one week to give more colorless solid. After collection of X-ray data, both batches were combined and washed with methanol (2x1 mL) and diethyl ether (2 mL) before drying *in vacuo*. Yield: 0.3 g (480.56 g·mol^{-1}, 55 %) of colorless solid. ^{1}H NMR ($CDCl_3$, 500 MHz, 298 K): δ = 12.53 (d, ^3J = 12.2 Hz, 1H, N*H*), 7.48–7.45 (m, 3H, CH_{ar}), 7.41–7.38 (m, 4H, CH_{ar}), 2.45 (s, 3H, CH_3), 1.67 (s, 3H, CH_3) ppm. MS (EI, pos): *m/z* = 480 (**H_2L^{TerPh}**, 10 %). EA ($C_{30}H_{28}N_2O_4$, %): calc. C 74.98 H 5.87 N 5.83. found. C 75.07 H 5.63 N 5.90.

[Fe(L^{TerPh})(MeOH)$_2$]: **H_2L^{TerPh}** (0.12 g, 0.24 mmol, 1.0 Eq.) and iron(II) acetate (0.048 g, 0.27 mmol, 1.12 Eq.) were refluxed for one hour in methanol (15 mL) to give a red-brown solution. Solid was separated by cannula filtration and washed with methanol (2 mL) followed by drying *in vacuo*. Yield: 0.0040 g of red-brown solid. EA ($C_{32}H_{34}Fe_1N_2O_6$, 598.48 g·mol^{-1}, %): calc. C 64.22 H 5.73 N 4.68. found. C 64.98 H 4.80 N 4.94.

[Fe(L^{TerPh})(bpee)]$_n$: The filtrate obtained in the preparation of **[Fe(L^{TerPh})(MeOH)$_2$]** was taken to precipitate the coordination polymer. 1,2-Bis-(4-pyridyl)-ethylene (0.10 g, 0.55 mmol) was set under Ar atmosphere and the filtrate solution was added *via* canula. An immediate color change was observed followed by the precipitation of dark blue solid, which was isolated by filtration (P4) after a few days and washed with methanol (2x3 mL) and dried *in vacuo*. Yield: 0.023 g (716.62 g·mol^{-1}) of dark-blue solid.

Acknowledgements

Financial support from the University of Bayreuth, the BayNAT program, and the SFB840 is gratefully acknowledged. We thank Dr. Ulrike Lacher for measuring the mass spectra. Open access funding enabled and organized by Projekt DEAL.

Conflict of Interest

The authors declare no conflict of interest.

Keywords: Schiff base · Iron · Spin crossover · Magnetic properties · Terphenyl

[1] L. Cambi, L. Szegö, *Ber. dtsch. Chem. Ges. A/B* **1931**, *64*, 2591–2598.
[2] a) P. Gütlich, *Eur. J. Inorg. Chem.* **2013**, *2013*, 581–591; b) M. A. Halcrow (Ed.) *Spin-Crossover Materials*, John Wiley & Sons Ltd, Chichester **2013**; c) P. Gütlich, H. Goodwin (Eds.) *Topics in Current Chemistry, 233–235*, Springer Berlin/Heidelberg **2004**.
[3] M.-L. Boillot, B. Weber, *C. R. Chim.* **2018**, *21*, 1196–1208.
[4] a) M. A. Halcrow, *Dalton Trans.* **2020**, *49*, 15560–15567; b) A. B. Gaspar, B. Weber, in: *Molecular Magnetic Materials* (Eds.: B. Sieklucka, D. Pinkowicz), Wiley-VCH Verlag GmbH & Co. KGaA, Weinheim, Germany **2017**, 231–252.
[5] P. Gütlich, A. Hauser, H. Spiering, *Angew. Chem. Int. Ed.* **1994**, *33*, 2024–2054; *Angew. Chem.* **1994**, *106*, 2109–2141.
[6] P. Gütlich, A. Hauser, H. Spiering, *Angew. Chem.* **1994**, *106*, 2109–2141; *Angew. Chem. Int. Ed.* **1994**, *33*, 2024–2054.
[7] a) J. A. Real, A. B. Gaspar, M. C. Munoz, *Dalton Trans.* **2005**, 2062–2079; b) P. Gütlich, V. Ksenofontov, A. B. Gaspar, *Coord. Chem. Rev.* **2005**, *249*, 1811–1829.
[8] J.-F. Letard, *J. Mater. Chem.* **2006**, *16*, 2550–2559.
[9] a) P. Gütlich, in: *Structure & Bonding, Vols. 44* (Eds.: R. Bau, P. Gütlich, R. G. Teller), Springer Berlin Heidelberg, Berlin, Heidelberg **1981**, 83–195; b) K. Senthil Kumar, Y. Bayeh, T. Gebretsadik, F. Elemo, M. Gebrezgiabher, M. Thomas, M. Ruben, *Dalton Trans.* **2019**, *48*, 15321–15337; c) H. L. Feltham, A. S. Barltrop, S. Brooker, *Coord. Chem. Rev.* **2017**, *344*, 26–53.
[10] K. Senthil Kumar, M. Ruben, *Coord. Chem. Rev.* **2017**, *346*, 176–205.
[11] A. Enriquez-Cabrera, A. Rapakousiou, M. Piedrahita Bello, G. Molnár, L. Salmon, A. Bousseksou, *Coord. Chem. Rev.* **2020**, *419*, 213396.
[12] a) E. Coronado, *Nature Rev. Mater.* **2020**, *5*, 87–104; b) G. Molnár, L. Salmon, W. Nicolazzi, F. Terki, A. Bousseksou, *J. Mater. Chem. C* **2014**, *2*, 1360–1366; c) J. Linares, E. Codjovi, Y. Garcia, *Sensors* **2012**, *12*, 4479–4492.
[13] H. J. Shepherd, C. M. Quintero, G. Molnár, L. Salmon, A. Bousseksou, in: *Spin-Crossover Materials* (Ed.: M. A. Halcrow), John Wiley & Sons Ltd, Chichester **2013**, 347–373.
[14] a) K. Cook, J. Laurence, R. Kulmaczewski, R. Mohammed, S. Dudley, S. A. Barrett, M. A. Little, R. J. Deeth, M. A. Halcrow, *Angew. Chem. Int. Ed.* **2016**, *55*, 4327–4331; *Angew. Chem.* **2016**, *128*, 4399–4403; b) D. C. Ashley, E. Jakubikova, *Inorg. Chem.* **2018**, *57*, 9907–9917; c) S. C. C. van der Lubbe, P.

Vermeeren, C. Fonseca Guerra, F. M. Bickelhaupt, *Chem. Eur. J.* **2020**.
[15] S. Schönfeld, W. Bauer, S. Thallmair, G. Hörner, B. Weber, *Z. Anorg. Allg. Chem.* **2021**, *647*, 905–914.
[16] a) E. Collet, P. Guionneau, *C. R. Chim.* **2018**, *21*, 1133–1151; b) S. Brooker, *Chem. Soc. Rev.* **2015**, *44*, 2880–2892; c) M. A. Halcrow, *Chem. Lett.* **2014**, *43*, 1178–1188; d) J. Weihermüller, S. Schlamp, W. Milius, F. Puchtler, J. Breu, P. Ramming, S. Hüttner, S. Agarwal, C. Göbel, M. Hund et al., *J. Mater. Chem. C* **2019**, *7*, 1151–1163; e) K. Dankhoff, C. Lochenie, F. Puchtler, B. Weber, *Eur. J. Inorg. Chem.* **2016**, *2016*, 2136–2143.
[17] W. Bauer, C. Lochenie, B. Weber, *Dalton Trans.* **2014**, *43*, 1990–1999.
[18] B. Weber, *Coord. Chem. Rev.* **2009**, *253*, 2432–2449.
[19] B. Weber, E.-G. Jäger, *Eur. J. Inorg. Chem.* **2009**, *2009*, 465–477.
[20] a) J. Weihermüller, S. Schlamp, B. Dittrich, B. Weber, *Inorg. Chem.* **2019**, *58*, 1278–1289; b) S. Schlamp, P. Thoma, B. Weber, *Eur. J. Inorg. Chem.* **2012**, *2012*, 2759–2768; c) S. Schlamp, P. Thoma, B. Weber, *Chem. Eur. J.* **2014**, *20*, 6462–6473.
[21] H. Kurz, K. Schötz, I. Papadopoulos, F. W. Heinemann, H. Maid, D. M. Guldi, A. Köhler, G. Hörner, B. Weber, *J. Am. Chem. Soc.* **2021**, *143*, 3466–3480.
[22] C. Lochenie, K. G. Wagner, M. Karg, B. Weber, *J. Mater. Chem. C* **2015**, *3*, 7925–7935.
[23] a) D. M. Gampe, S. Schramm, F. Nöller, D. Weiß, H. Görls, P. Naumov, R. Beckert, *Chem. Commun.* **2017**, *53*, 10220–10223; b) B. A. D. Neto, A. S. Lopes, M. Wüst, V. E. Costa, G. Ebeling, J. Dupont, *Tetrahedron Lett.* **2005**, *46*, 6843–6846.
[24] L. Wolf, E.-G. Jäger, *Z. Anorg. Allg. Chem.* **1966**, *346*, 76–91.
[25] B. Weber, E. Kaps, J. Weigand, C. Carbonera, J.-F. Létard, K. Achterhold, F. G. Parak, *Inorg. Chem.* **2008**, *47*, 487–496.
[26] K. L. Taft, S. J. Lippard, *J. Am. Chem. Soc.* **1990**, *112*, 9629–9630.
[27] W. Bauer, T. Ossiander, B. Weber, *Z. Naturforsch. B* **2010**, *2010*, 323–328.
[28] a) T. Steiner, G. R. Desiraju, *Chem. Commun.* **1998**, 891–892; b) T. Steiner, *Angew. Chem. Int. Ed.* **2002**, *41*, 48–76; *Angew. Chem.* **2002**, *114*, 50–80.
[29] R. Ketkaew, Y. Tantirungrotechai, P. Harding, G. Chastanet, P. Guionneau, M. Marchivie, D. J. Harding, *Dalton Trans.* **2021**, *50*, 1086–1096.
[30] S. Schlamp, P. Thoma, T. Bauer, R. Kempe, B. Weber, *Z. Anorg. Allg. Chem.* **2013**, *639*, 1763–1767.
[31] B. Weber, E.-G. Jäger, *Z. Anorg. Allg. Chem.* **2009**, *635*, 130–133.
[32] W. Bauer, W. Scherer, S. Altmannshofer, B. Weber, *Eur. J. Inorg. Chem.* **2011**, 2803–2818.
[33] K. Dankhoff, C. Lochenie, B. Weber, *Molecules* **2020**, *25*, 581.
[34] S. Schönfeld, G. Hörner, F. W. Heinemann, A. Hofmann, R. Marschall, B. Weber, *Z. Anorg. Allg. Chem.* **2021**, *647*, 295–305.
[35] H. Kurz, J. Sander, B. Weber, *Z. Anorg. Allg. Chem.* **2020**, *646*, 800–807.
[36] R. Nowak, W. Bauer, T. Ossiander, B. Weber, *Eur. J. Inorg. Chem.* **2013**, *2013*, 975–983.
[37] W. Bauer, T. Pfaffeneder, K. Achterhold, B. Weber, *Eur. J. Inorg. Chem.* **2011**, 3183–3192.
[38] D. N. Bowman, E. Jakubikova, *Inorg. Chem.* **2012**, *51*, 6011–6019.
[39] M. Reiher, O. Salomon, B. Artur Hess, *Theor. Chem. Acc.* **2001**, *107*, 48–55.
[40] B. Weber, R. Betz, W. Bauer, S. Schlamp, *Z. Anorg. Allg. Chem.* **2011**, *637*, 102–107.
[41] L. Claisen, *Justus Liebigs Ann. Chem.* **1897**, *297*, 1–98.
[42] H. G. O. Becker, *Organikum.* Organisch-chemisches Grundpraktikum, 19th ed., Johann Ambrosius Barth, Berlin **1993**.
[43] G. Sheldrick, *Acta Crystallogr. Sect. A* **2014**, *70*, C1437-C1437.
[44] G. M. Sheldrick, *Acta Crystallogr. Sect. C* **2015**, *71*, 3–8.
[45] L. J. Farrugia, *J. Appl. Crystallogr.* **2012**, *45*, 849–854.
[46] C. F. Macrae, I. Sovago, S. J. Cottrell, P. T. A. Galek, P. McCabe, E. Pidcock, M. Platings, G. P. Shields, J. S. Stevens, M. Towler et al., *J. Appl. Crystallogr.* **2020**, *53*, 226–235.
[47] A. L. Spek, *J. Appl. Crystallogr.* **2003**, *36*, 7–13.
[48] G. A. Bain, J. F. Berry, *J. Chem. Educ.* **2008**, *85*, 532.
[49] K. Lagarec, D. G. Rancourt, *Recoil, mössbauer spectral analysis software for windows 1.0*, Department of Physics, University of Ottawa, Canada **1998**.
[50] F. Neese, *WIREs Comput. Mol. Sci.* **2012**, *2*, 73–78.
[51] A. Schäfer, H. Horn, R. Ahlrichs, *J. Chem. Phys.* **1992**, *97*, 2571–2577.
[52] Becke, *Phys. Rev. A* **1988**, *38*, 3098–3100.
[53] V. N. Staroverov, G. E. Scuseria, J. Tao, J. P. Perdew, *J. Chem. Phys.* **2003**, *119*, 12129–12137.
[54] a) L. Kletsch, G. Hörner, A. Klein, *Organometallics* **2020**, *39*, 2820–2829; b) R. Alrefai, G. Hörner, H. Schubert, A. Berkefeld, *Organometallics* **2021**, *40*, 1163–1177.
[55] S. Schönfeld, K. Dankhoff, D. Baabe, M.-K. Zaretzke, M. Bröring, K. Schötz, A. Köhler, G. Hörner, B. Weber, *Inorg. Chem.* **2020**, *59*, 8320–8333.
[56] a) R. M. Dickson, A. D. Becke, *J. Chem. Phys.* **1993**, *99*, 3898–3905; b) B. Miehlich, A. Savin, H. Stoll, H. Preuss, *Chem. Phys. Lett.* **1989**, *157*, 200–206.
[57] S. Grimme, J. Antony, S. Ehrlich, H. Krieg, *J. Chem. Phys.* **2010**, *132*, 154104.
[58] A. Klamt, G. Schüürmann, *J. Chem. Soc. Perkin Trans. 2* **1993**, 799–805.

Manuscript received: June 2, 2021
Revised manuscript received: July 16, 2021
Accepted manuscript online: July 19, 2021

